Available online at www.sciencedirect.com
ScienceDirect
Deep-Sea Research II 53 (2006) 2457–2476
DEEP-SEA RESEARCH PART II
www.elsevier.com/locate/dsr2

Sources of variability in Gulf of Maine circulation, and the observations needed to model it

James M. Pringle

142 Morse Hall, UNH, 39 College Str., Durham, NH 03824-3525, USA

Accepted 24 August 2006

Abstract

Variability in the circulation of coastal oceans must ultimately be driven by changes in the meteorological conditions that force currents in the coastal ocean, and by variability in the waters entering the coastal ocean from elsewhere. If a coastal ocean is to be understood and modeled accurately, the external forcing that drives the largest portions of the circulation variability must be observed adequately. Thus, some method of comparing the relative importance of various sources of circulation variability must be developed, so that there is confidence that the most important sources of variability are included in any analysis or modeling. This is done for variability in the time-integrated transport across a section in a coastal ocean.

The relative importance of various sources of circulation variability in the Gulf of Maine (GoM) are then quantified, with an emphasis on variability on timescales longer than tidal or weather-band timescales. In order to concentrate on interannual changes, the seasonal cycle is not included in estimates of variability. It is found that the variability forced by fluctuations in the winds and the volume of water entering from the Scotian Shelf to the GoM produce roughly comparable amounts of circulation variability. However, changes in the density structure of the GoM produce changes in time-integrated transport that are an order of magnitude larger, at least in the central GoM. The changes in the large-scale density gradients are governed by mixing processes in the Gulf and by changes in the water masses entering the GoM from the Scotian Shelf and the Northeast Channel. Unless the heat, freshwater and volume transport of the waters entering the GoM are routinely observed, numerical models will fail to capture much of the variability in the circulation of the Gulf. An analysis is given of the minimal set of observations needed to allow numerical models of the GoM to resolve adequately the true variability in the circulation.

Keywords: USA; Gulf of Maine; Ocean observing; Coastal circulation

0. Introduction

There is an increased desire to understand the sources of interannual variability in the ecosystems of coastal oceans, and thus of the variability of the ocean circulation that governs these ecosystems. In order to understand the circulation variability, the relative importance of the sources of this variability must be understood. In the analysis below, the relative importance of various sources of circulation variability in the Gulf of Maine (GoM) is quantified.

The transports driven by the currents in the GoM control many important ecological processes,

E-mail address: jpringle@cisunix.unh.edu.

0967-0645/$ - see front matter © 2006 Elsevier Ltd. All rights reserved.
doi:10.1016/j.dsr2.2006.08.015

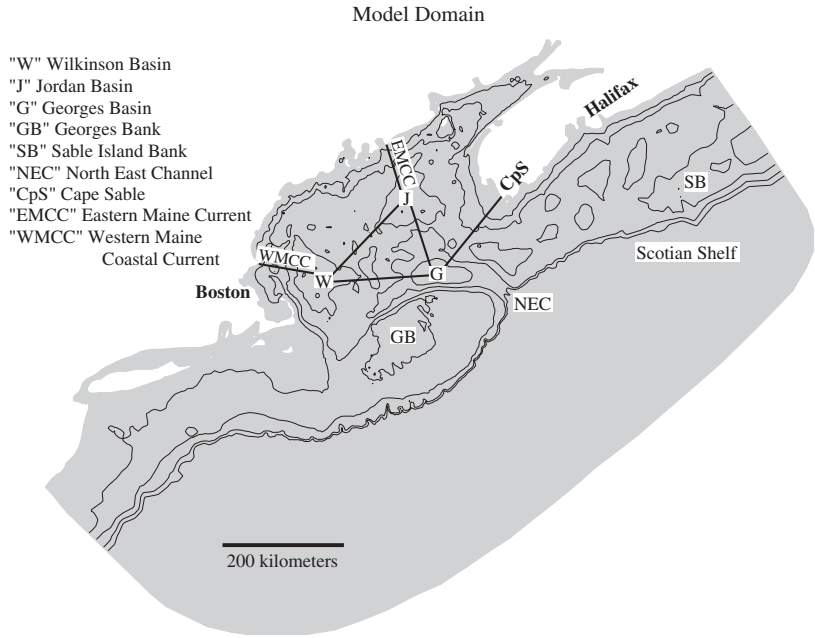

Fig. 1. The domain of the FVCOM model, including the 300, 200, 100 and 50 m isobaths. Indicated are the sections across which transport is calculated, and the major basins and other features of the Gulf of Maine and Scotian Shelf.

and the examination of circulation variability below will focus on time and space scales of broad ecological interest. The transport of near-surface waters from the northeast GoM to the southwest and then onto Georges Bank move copepods from the Gulf where they can reproduce successfully onto the Bank, where they are food for economically important larval fish (Hannah et al., 1998). Transport along the coast of Maine can move harmful algal bloom species along the coast and drive toxic blooms in the western GoM (Franks and Anderson, 1992). Many economically important benthic species have planktonic larval stages that are dispersed by the currents. The population dynamics and the retention of these populations are thus strongly influenced by the variability in the currents, integrated over the time the larvae are in the plankton (Byers and Pringle, 2006). In each of these three examples, what matters is not the instantaneous value of the currents, but the Lagrangian pathways of the planktonic stage over the ecologically relevant timescales of weeks to several months to a year. These Lagrangian motions are strongly affected by the large-scale circulation in the GoM integrated over these ecologically relevant timescales (Johnson et al., 2006). Thus it is the variability in the largest spatial scale of circulation—the transport across sections connecting the three deep basins of the GoM to each other and the coast—that will be quantified (Fig. 1). In order to focus on changes from one year to the next, variability due to the annual cycles in circulation will be removed from the analysis, as will motions on tidal timescales.

The GoM is a semi-enclosed sea, bounded to the northeast by Nova Scotia and New Brunswick, to the southwest by the Massachusetts coast, and offshore by large shallow banks and shelves, including Georges Bank, Nantucket Shoals, and the Scotian Shelf (Fig. 1). At depths below 70 m, the only connections to the outside ocean are through relatively narrow channels, the Northeast Channel (NEC) and a mid-shelf channel entering from the Scotian Shelf (SS). In the GoM, there are three large deep basins, Georges, Jordan and Wilkinson Basins.

The circulation in the GoM and its variability are ultimately forced by the flow through alongshore and offshore boundaries, the heat and freshwater transported into the domain by these flows, the winds, and by the surface fluxes of heat and water. However, to quantify fully the variability driven by the boundary forcing, it would be necessary to have accurate information on the variability of the water masses entering the GoM. Unfortunately, the variability of the temperature and salinity transported through the open boundaries on the SS and

through the NEC is poorly constrained. Thus, the examination of the sources of circulation variability will be constrained to include variability forced by winds, the changes in the volume of water entering the GoM from the SS, and the variability in the large-scale density field in the Gulf of Maine. This later source of variability will implicitly include the effects of changing heat and freshwater transport into the GoM from the SS and NEC, as well as surface buoyancy fluxes, river inputs, and wind-driven mixing of density. A brief analysis of the origins of the variability in density-driven circulation will then be given. Variability forced by changes in the volume of water entering the NEC will not be considered, because in the modeling described below, it was found that the inflow through the NEC was controlled by the winds, SS inflow, and density gradients in the GoM (cf. Ramp et al., 1985, Appendix). It was not found to be possible to change the inflow through the NEC independently of these quantities. Variability driven by radius of deformation scale features in the hydrographic field, such as eddies formed by baroclinic instabilities (e.g., Vermersch et al., 1979), will not be included in this analysis, thus making the estimates of variability presented here a lower limit on the actual variability. Likewise, due to lack of adequate data, the impact of warm-core Gulf Stream rings on the circulation will not be included, except insofar as they modify the density in the GoM by altering the water properties entering it.

This partitioning of sources of variability into wind, boundary inflow transport, and hydrographic forced variability introduces some ambiguity. Winds and changes in the volume of water entering the GoM can alter the hydrography in the GoM, and care must be taken to prevent double counting sources of variability. To avoid this, the analysis of these sources of variability will be limited to the sub-inertial currents they drive directly. This partitioning of sources of variability can be made because the timescales over which the GoM first responds to a change in winds or inflow volume are a few days or less, while the effects of the change in currents on density occurs on advection timescales. At least for density changes caused by the alongshore advection of density, these advection timescales are much longer, with $O(10\,cm\,s^{-1})$ flows and distances of many hundreds of kilometers leading to timescales of weeks to several months. The analysis below will become suspect in locations where density advection modifies the baroclinic flow field on weatherband timescales, e.g., near the coast where a few days of upwelling-favorable winds can create an upwelling front.

It will be found that most of the variability relevant to the transport on timescales of several months or longer is not captured in most current models, not because of any failures of the models, but because of the inadequacies of our observational schemes that initialize and provide the boundary conditions for our models. A minimal set of ongoing observations needed to allow models to capture the true variability of the Gulf will be defined.

1. Methods

1.1. Quantifying sources of variability

1.1.1. Comparing two sources of variability

In order to compare the relative importance of various sources of circulation variability in the ocean, it is necessary to examine how circulation variability of a known magnitude and timescale affects the transport across a section when averaged or integrated over a fixed time interval. If a fluctuating forcing produces a flow with a decorrelation timescale of τ, and induces a transport whose standard deviation (SD) is σ_V across the section, then over a single random fluctuation of the forcing it can be expected to drive a net time-integrated transport that scales as $\tau\sigma_V$. After N random fluctuations of this magnitude, the SD of the net time-integrated transport is $N^{1/2}\tau\sigma_V$ (derived from Bevington and Robinson, 1992). The random fluctuations decorrelate on a timescale τ, so $N = T/\tau$, where T is the time over which the transport is integrated. Thus the SD of the transport integrated over a time T is

$$\text{SD of time-integrated transport} = (\text{Dispersion}) \times T^{1/2}, \quad (1)$$

where the dispersion is defined as

$$\text{Dispersion} = \tau^{1/2}\sigma_V. \quad (2)$$

Thus for timescales longer than τ, the relative contribution of two uncorrelated random processes to the SD of the integrated or mean transport through a section will scale linearly with their dispersion, as defined in (2). On timescales less than each τ, the relative contribution of each processes

would scale linearly with their σ_V. Implicit in this discussion is an assumption that the ocean responds linearly to the two sources of variability—e.g., that changes in the ocean caused by one source of variability do not effect the magnitude of the oceans response to the other source of variability.

1.1.2. Relating transport variability to forcing variability

In order to calculate the transport dispersion defined in (2), it is necessary to relate the strength and decorrelation timescale of the ocean transport to the strength and decorrelation timescale of the various forcing mechanisms of interest.

As a simple model of ocean dynamics, consider a transport which responds linearly to some forcing F, with a linear first-order friction of strength λ:

$$\frac{\partial U}{\partial t} = F - \lambda U. \tag{3}$$

This is a good model of the depth-integrated alongshore current forced by an alongshore wind of infinite extent along a straight coast (e.g., Dever, 1997), and is a reasonable model of many forcing processes in the coastal ocean which at first accelerate an alongshore or along-isobath flow until some other mechanism retards the flow. In order to understand the decorrelation timescale of U, it is useful to examine the case in which F is a white-noise process, and thus the expected value of the Fourier transform of F, $\hat{F}$, is a constant independent of the frequency ω and of some magnitude $\hat{F}_0$. Fourier transforming (3) allows us to write the spectra of the transport U:

$$\hat{U} = \frac{\hat{F}_0}{\mathrm{i}\omega + \lambda}. \tag{4}$$

From (4), the expected power-spectra of U can be calculated. From the convolution theorem (Bracewell, 1986), it can be shown that the Fourier transform of the power-spectra is the unnormalized lagged auto-correlation function, allowing the calculation of the auto-correlation function of U from (4) as a function of a lag t_{lag}

$$\text{Auto-correlation of } U = \exp(-\lambda|t_{\mathrm{lag}}|) \tag{5}$$

from which it can be seen that the decorrelation timescale of this simple model ocean when forced by white-noise forcing scales as λ^{-1}. This can be explained by noting that in this simple system U is a low-pass filtered version of F. On timescales longer than λ^{-1}, U is proportional to F. On timescales less than λ^{-1}, U is proportional to the time-integral of F. If F has a decorrelation timescale greater than λ^{-1}, and thus has little energy in periods less than λ^{-1}, U will be roughly proportional to F.

From this it can be seen that if the response timescale of the ocean to forcing λ^{-1} is greater than the timescale of the forcing, then the decorrelation timescale of the transport is set by λ^{-1}, while if λ^{-1} is less than the decorrelation timescale of the forcing it is the decorrelation timescale of the forcing which sets the decorrelation timescale of the transport.

1.1.3. Calculating timescales τ from observations

The decorrelation timescale of a time series can be estimated from the integral decorrelation timescale as discussed by Davis (1976). For a finite length of discrete time data of length greater than l taken at an interval of Δt, the timescale can be estimated using l lags of the data with

$$\tau = \sum_{n=-l}^{l} \left(l - \frac{|n|}{l}\right) r(n\Delta t)\Delta t, \tag{6}$$

where $r(n\Delta t)$ is the lagged auto-correlation of the data lagged by a time $n\Delta t$. The maximum lag l must be greater than the actual decorrelation timescale for this to be valid. Where data are missing, it is not included in the lagged correlation. Because $r(n\Delta t)$ becomes poorly defined as n approaches the record length, τ is estimated for the value of l that produces the largest τ, and l is limited to half the record length.

In all calculations below, the seasonal cycle and any super-inertial and tidal energy is removed from the data, and the time series were detrended.

1.2. Numerical modeling

To estimate the variability in GoM transport driven by the fluctuating winds or SS inflow, a numerical model was used to estimate the transport driven by these fluctuating forcings. Model runs were used to estimate the time it takes the GoM circulation to reach a nearly steady state circulation after a change in winds or SS inflow (the "response timescale"). The numerical model runs were also used to estimate the transfer coefficients between the wind or the SS inflow and the transport in the GoM on timescales longer than the response timescale, and were used to examine the linearity of the oceanic response to forcing on timescales longer

than the response timescale. The GoM was numerically modeled with the Finite-Volume Coastal Ocean Model (FVCOM). FVCOM is a free-surface, hydrostatic, primitive-equation numerical model with an unstructured triangle-based finite element mesh (Chen et al., 2003). Descriptions of the model configuration, boundary conditions, model runs, and forcing are given in the Appendix.

1.3. Hydrographic data

The hydrographic data used in the analysis below were taken from the Bedford Institute of Oceanography (BIO) hydrographic database, and include all data from 1970 to 2003. These data come from a large number of sources, including National Marine Fisheries Surveys, Canadian and US Government surveys, and US and Canadian academic sources. BIO has endeavored to include all publicly available hydrographic data in this region in its database. Data were removed if they extended below the water depth given by the USGS 15' GoM bathymetric product (Roworth and Signell, 1998).

2. Wind-driven variability

The monthly mean winds in the GoM are persistently upwelling favorable as defined by the Maine coast (55°T), but the SD of the windstress averaged over a single month is much larger than the climatological mean windstress for that month, indicating that in any specific month there is a large probability that the month's averaged winds will not even be of the same sign as the climatological mean for that month (Fig. 2, from the NCEP reanalysis of Kalnay et al. (1996) at 42.8°N, 67.5°W for the years 1970–2003). Variability is largely isotropic and is much stronger in the winter and early spring (Fig. 2; Manning and Strout, 2001). The decorrelation times of the windstress varies less from season to season than do the winds themselves, with a decorrelation timescale of 2.1 days in the winter and a slightly larger 2.4 days in the summer for the alongshore winds. (More details on the winds, and their spatial scales, can be found in the Appendix.)

The response of the GoM to these winds has been studied extensively, both observationally (Brown, 1998; Noble et al., 1985) and numerically (Greenberg et al., 1997; Naimie, 1996). The response of the GoM is strongest to winds along the Maine coast, and weaker to winds across the Maine Shelf (Noble et al., 1985; Greenberg et al., 1997). Upwelling-favorable winds (defined here and below with respect to the Central Maine coast) and offshore winds drive sea-level setdown over the entire GoM, and the pressure gradients so formed drive substantial currents. The current and pressure response to the winds is rapid, with roughly 80% of the response observed to occur within 36 h (Brown, 1998), and the response is observed to be very nearly linear to windstress, both with respect to magnitude and direction (Noble et al., 1985). These results are consistent with those obtained with the numerical model (see Appendix). The modeled response of the GoM to winds does not change greatly by season, suggesting that typical changes in the density field do not significantly alter the response of the GoM to winds. Since the timescale of the response of the GoM to the winds is less than the decorrelation timescale of the winds, the timescale of the winds shall be used to estimate the dispersion of the wind-driven flows.

Consistent with observations, FVCOM and other numerical models of the region find that an alongshore (55°T) upwelling-favorable wind drives an offshore surface Ekman flux (Fig. 3), which causes a sea-level setdown that drives a largely barotropic flow along the shelf, through the NEC (Ramp et al., 1985), along the ridge between Wilkinson and Jeffreys Basins and to the west of Wilkinson Basin, along the Maine coast to Nova Scotia and out the SS (cf., Greenberg et al., 1997). The wind-forced flow is roughly along lines of constant depth. The wind-forced depth-averaged transport across the section between Georges Basin and Wilkinson Basin is relatively small in the numerical model, as the geostrophic transport across this section is nearly equal and opposite to the Ekman transport across the section.

Similarly, an offshore wind (145°T) drives a surface Ekman transport to its right in FVCOM, to the southwest. There is a divergence of this surface transport when it leaves the coast of Nova Scotia and a convergence when it encounters the north/south trending Massachusetts and New Hampshire coasts. These divergences and convergences are fed by Ekman transports from the SS and by a geostrophic return flow that travels northwestward along the Maine coast.

In Table 1, the dispersion of the wind-driven transport is shown for the depth-averaged transport across the standard sections. These dispersion results are valid for times greater than the decorrelation timescale of the winds for each season. The alongshore wind-driven dispersion is large through

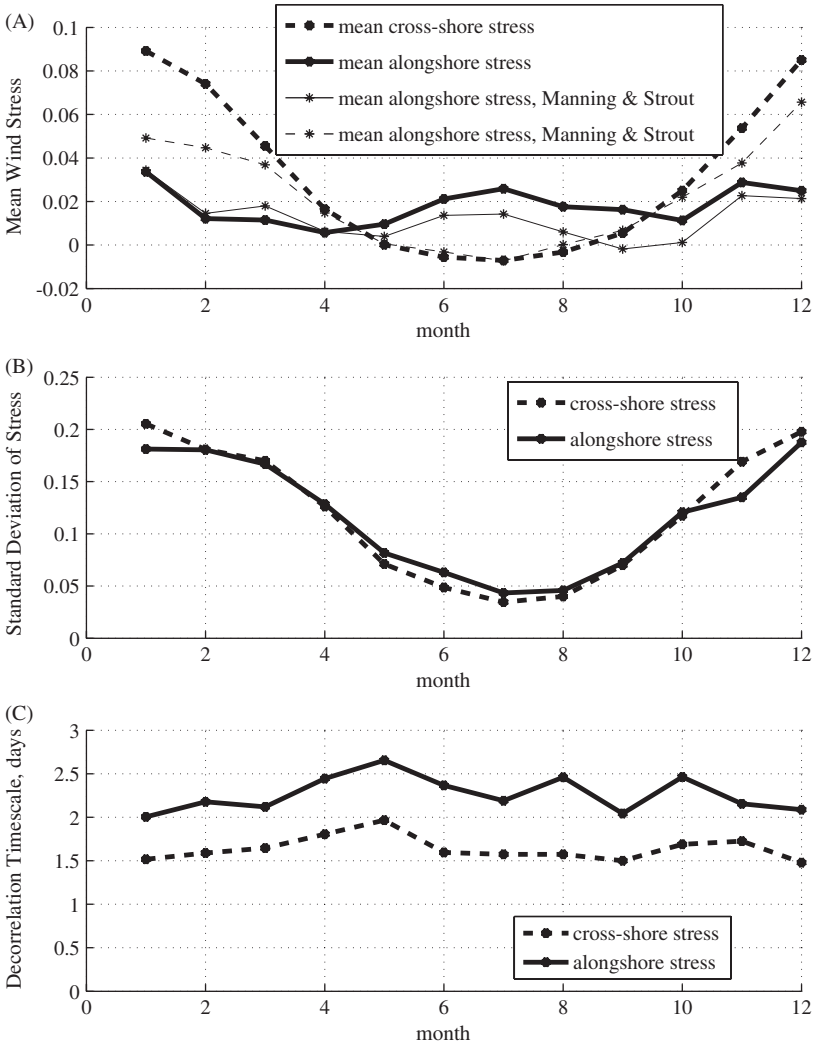

Fig. 2. Monthly windstress statistics from the 1970 to 2003 NCEP reanalysis and from Manning and Strout (2001). (A) Monthly mean winds in the alongshore (55°T) and cross-shore (145°T) direction, as defined by the coast of Maine. (B) The standard deviation of the NCEP wind stresses. (C) Decorrelation timescales of windstress by month.

the NEC, across the central GoM, along the EMCC and WMCC, and out the SS. This dispersion is much less in the summer than in the winter, as would be expected from the seasonal change in the variance of the winds (Fig. 2). The transport dispersion driven by the cross-shelf winds is again as expected from the model-derived depth-averaged wind-driven currents shown in Fig. 2, with the cross-shore winds forcing less transport dispersion than alongshore winds in most sections.

3. Inflow-driven variability

The transport along the SS is dominated by alongshore currents in thermal wind balance with cross-shelf density gradients (Smith and Schwing, 1991; Loder et al., 2003). The effect on the circulation in the GoM of the volume of water entering from the SS and driven by cross-shelf density gradients is quantified in this section—the effects of changes in the heat and freshwater transported into the GoM from the SS will be considered briefly in the next section and in the discussion. The effects of SS transport fluctuations impact the entire model domain quickly, within a few days, consistent with the observed coastal trapped wave speeds on the SS of 6.5 $m\,s^{-1}$ or faster (Schwing, 1989), while the different water masses entering the SS shelf affect the GoM on a slower advective timescale set by the O(10) $cm\,s^{-1}$ mean

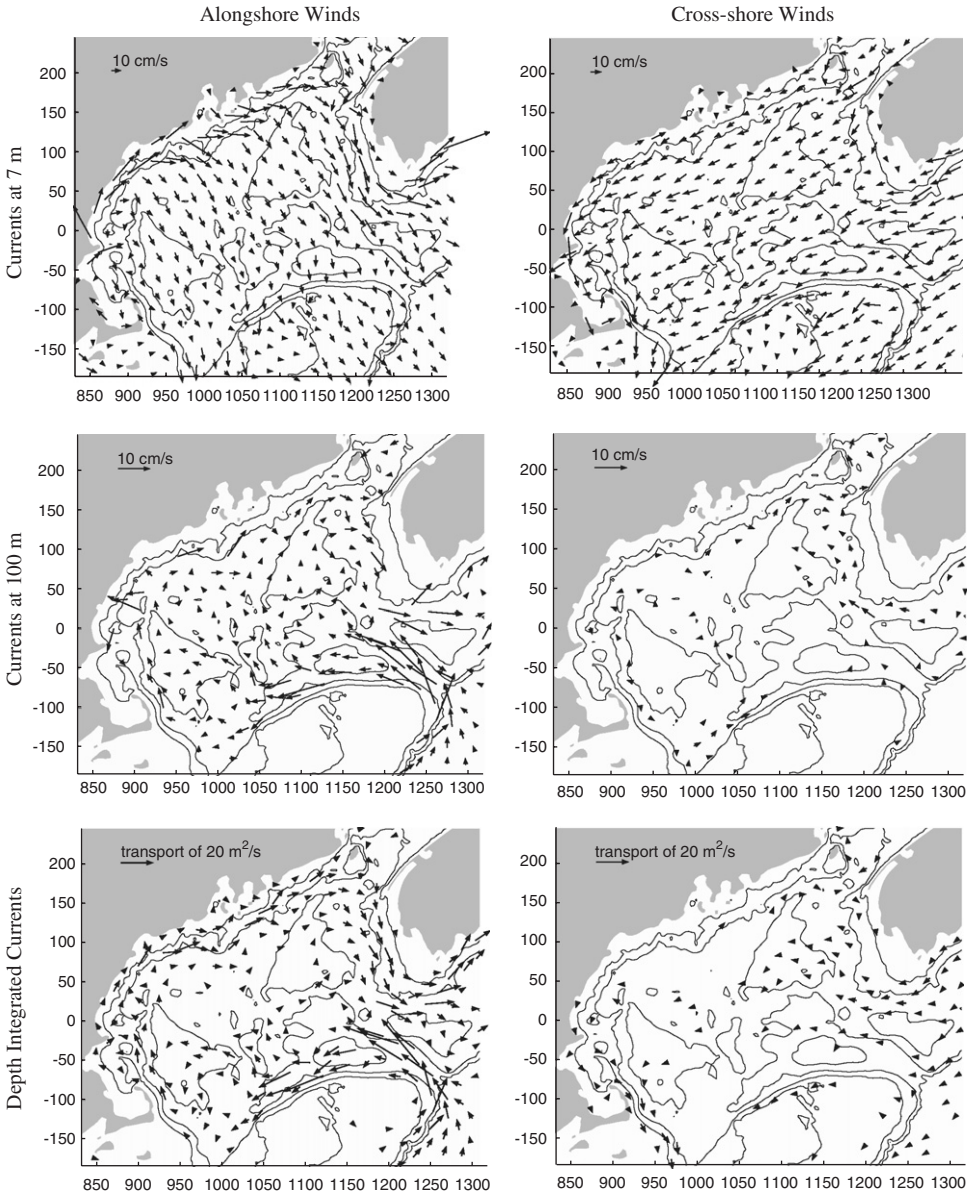

Fig. 3. The oceanic response to 10 m s^{-1} alongshore (left) and cross-shore (right) winds at (top) 7 m, (middle) 100 m, and (bottom) the depth-integrated response. Alongshore and cross-shore are defined with respect to the Maine coast; the response is found from the difference between model runs with no winds and model runs in which the winds had been blowing long enough that the circulation has become nearly steady. Arrows are not shown for currents of less than 0.75 cm s^{-1} and transports per unit length of less than 2 m^2 s^{-1}. Wind converted to stress following Large and Pond (1981).

currents (Smith et al., 2001). The response of the GoM to changes in SS inflow does not vary significantly in model runs made with different monthly mean hydrographies, suggesting that the response is not significantly altered by realistic changes in the Gulf's hydrography. (The changes in SS inflow driven by winds whose spatial scales are large enough to include the GoM and the SS are included in the analysis in the previous section—see the Appendix for details.)

The variability of the inflow along the SS is quantified from three different data sets—the repeated occupations of a cross-shelf section at Halifax, Nova Scotia (Loder et al., 2003), an analysis of this and other hydrographic data gathered by the BIO, and current meter data

Table 1
Dispersion as calculated from (2) for the sections defined in Fig. 1

	τ	CpS-G	G-J	EMCC	J-W	WMCC	W-G
Alongshore winds							
March	2.10	161.3	75.3	236.6	103.9	132.8	28.6
August	2.50	53.1	41.6	94.7	46.5	48.2	5.0
Cross-shore winds							
March	1.60	100.3	78.0	22.3	34.6	56.9	43.4
August	1.50	33.2	25.2	8.0	10.9	18.9	14.4
Scotian Shelf variability							
March	10.00	144.6	44.8	99.8	78.7	21.1	123.6
August	10.00	89.7	17.4	72.3	60.0	12.4	77.4
Hydrographic variability							
Winter	(see text)		738		700*		1336
Summer	(see text)		616		428*		916

Starred estimates are unreliable due to poor estimates of decorrelation timescale. Decorrelation timescale in days, dispersion in $10^6\,m^3\,s^{-12}$.

*Estimate not robust due to uncertainty in decorrelation timescale.

gathered as part of the Canadian Atlantic Storms Program (CASP) from December 1985 to April 1986 (Anderson and Smith, 1989).

The analysis of Loder et al. (2003) divides the alongshore transports into "inner" and "outer" portions, the former from the shore to the 244-m isobath in a deep mid-shelf basin, the latter from that isobath across an offshore bank to the shelf break at 341 m. Experimentation with FVCOM indicates that little of the transport in the "outer" section enters the GoM, and alterations made to the outer transport by changing the upstream boundary conditions have negligible effects on the GoM circulation. Thus attention will be focused below on the variability of the transport in the "inner" section of Loder et al. (2003), and the effects of changes in inflow through the model's open boundary are calibrated by its effect on the Halifax "inner" transport.

The SD of the inner-shelf transport as determined from 1955 to 1970 hydrographic sections with a level of no motion at the bottom is 0.24 Sv for the entire year (data courtesy of C. Hannah, from the analysis of Loder et al., 2003). The variability is 48% greater in the winter, with a SD of 0.28 Sv for December through April and 0.19 Sv from July to September.

Unfortunately, the Loder et al. (2003) data are too widely spaced in time to calculate a decorrelation timescale—so to do so, current meter data from the CASP program of the winter of 1985–1986 were used (data courtesy of Smith are described in Anderson and Smith, 1989). A comparison was made between the vertical shear in the sub-inertial alongshore currents between the depths of 16 and 110 m on the 165-m isobath and the vertical shear predicted from thermal wind and the sub-inertially filtered cross-shelf density gradient calculated at 70-m depth between the 100- and 220-m isobaths, 36 km apart. The correlation between the thermal-wind shear and the observed shear was $r = 0.8$, and the magnitude of the shears differed by only 6% (cf., Anderson and Smith, 1989). The decorrelation timescale was about 10 days for both the cross-shelf density gradient and the vertical shear in the sub-inertial alongshore currents. Of course, these calculations are only valid for the one winter over which the CASP data exist.

To confirm the validity of the decorrelation time estimate, all hydrographic data from the BIO hydrographic database between 43.8–45°N and 63.8–62.5°W from 1970 to 2003 were used to calculate a time series of cross-shelf density gradients. Any data taken within 2 days of each other were assumed to have been taken simultaneously. The density observations were differenced from the mean cross-shore density gradient at 50, 70 and 100 m, and all data in the 2-day window were used to compute a cross-shelf density gradient anomaly time series at each depth. To estimate robustly a decorrelation time from this unevenly spaced time series, the data were broken into sets of pairs of data separated by a fixed time—e.g., all pairs of data 2–7 days apart, 7–14 days apart, ad infinitum—and the number of pairs both above or below the median density were recorded. If this number was greater than would be expected by chance, as judged by the test for a fair coin toss at the 95% level, the time series was considered auto-correlated at the tested lag. With this test, there is significant correlation for lags of between 2 and 8 days, while there is none on timescales longer, except for a weak indication of a seasonal cycle. This result does not change if the summer or winter data are excluded. Thus the results of the analysis of the CASP data seem robust. Because the decorrelation time of the inflow transport is longer than the timescale of the GoM response to the change in inflow, the former sets the decorrelation timescale used to estimate the dispersion.

The circulation induced in the GoM by a given inflow along the SS shelf is essentially identical in the summer and winter. Fig. 4 shows the effect of a

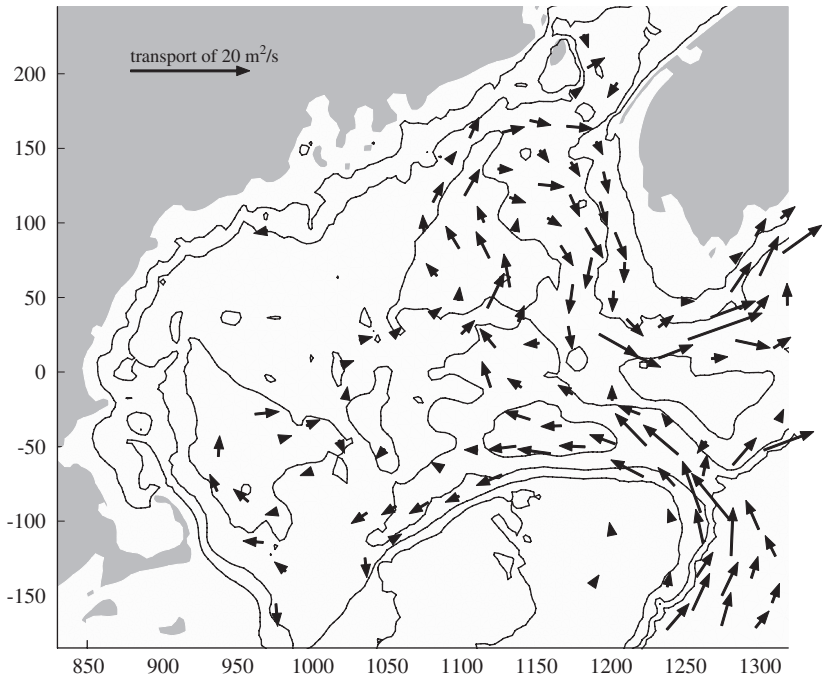

Fig. 4. Anomalous depth-integrated velocities forced by Scotian Shelf inflow for the month of March, for an anomalous reduction of Scotian Shelf inflow of 0.24 Sv, the standard deviation of the Inner Shelf Halifax transport from Loder et al. (2003) for the winter months.

decrease in the transport across the Halifax inner-shelf section of 0.24 Sv on the GoM circulation. The anomalous flows forced by a reduction in SS inflow are strikingly similar to the alongshore-wind-driven flows. Flow enters the GoM through the NEC, flows along the ridge between the basins, along the Eastern Maine coast, around Cape Sable and out the SS.

In Table 1, the transport dispersion driven by SS variability is seen to be somewhat greater than the wind-driven dispersion in the central and eastern GoM. This is not as much because of the greater strength of the currents the inflows force, but due to the longer timescales of the variability.

4. Density-driven variability

Near-surface geostrophic flows in the GoM are strongly driven by density gradients at depths below 100 m (e.g., Brown and Irish, 1992). The deep density structure can be clearly seen to strongly influence the surface circulation in Fig. 5. As will be shown below, these deep density gradients vary greatly from year to year, and thus are an important source of transport variability. However, changes in the internal density field are not an external source of variability affecting the ocean—they are instead the result of multiple processes that are either hard to quantify with available data (e.g., changes in the density of water entering the GoM) or processes that interact non-linearly (such as the interaction of wind- and cooling-driven vertical mixing). In this section, the effects of changes in the density field will be quantified, and in later sections the sources of density gradient variability will be discussed.

Unfortunately, the available density observations are insufficiently dense in space and time to be used to initialize the numerical model adequately, for the model needs a relatively widespread data coverage to model the circulation realistically. So instead of using the numerical model to estimate transport variability driven by changes in hydrography, the hydrography from the BIO hydrographic database will be used to estimate directly geostrophic transports between the three basins, Georges, Jordan and Wilkinson, and thus to determine the variability of these transports. The numerical model will only be used to check the dynamic consistency of assumptions about the level of no motion. Unfortunately, this method fails between the basins and the shore, where temporal and spatial variation of the density field are on shorter scales than in the basin interior, and so are not reliably resolved by the relatively sparse hydrographic data.

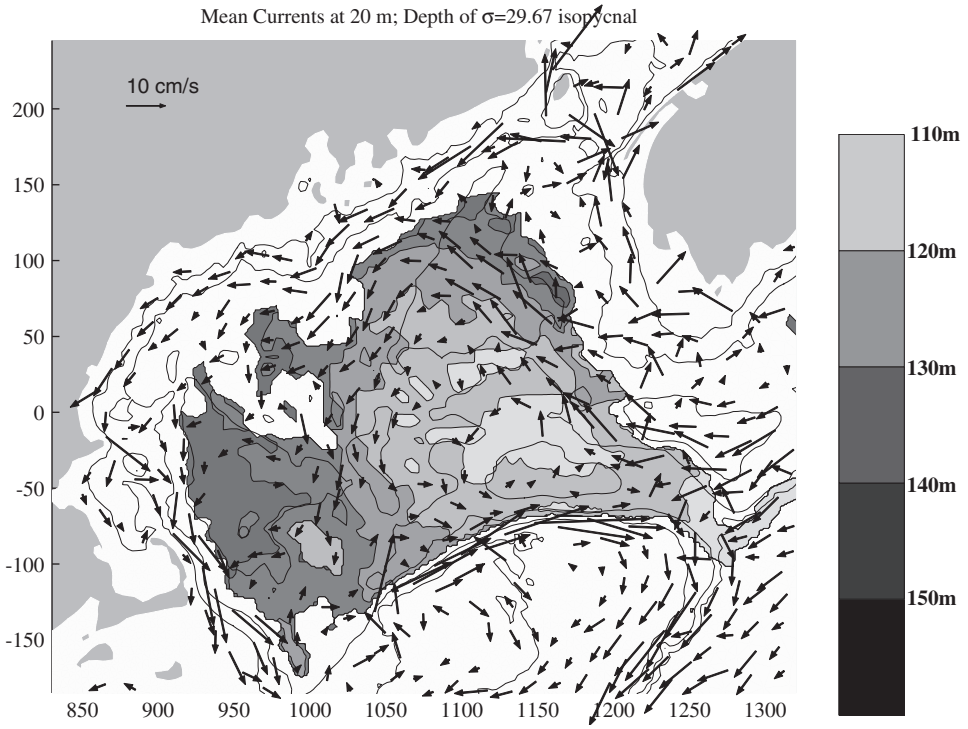

Fig. 5. Climatological depth of 29.67 σ isobath overlain by 20 m detided currents for the month of March, from FVCOM with no mean winds and no anomalous SS inflow. Both the currents and the isopycnal depth are calculated with the climatological density described by Chen et al. (2006).

In order to aggregate multiple density observations from multiple space and time points, three areas in the deep basins are chosen where the mean horizontal density gradients are weak, to reduce the aliasing of spatial gradients into a temporal signal. These three areas are shown in Fig. 6 and are defined by the 200-m isobaths around Wilkinson and Jordan Basins, and by the 200-m isobath of Georges Basin less a region near Georges Bank where there are large spatial gradients associated with tidal mixing (Chen et al., 1995). The data are then binned by quarter. This quarterly data are included in the analysis if the number of casts with both temperature and salinity data in a bin in a quarter year is equal to or greater than 4. The results presented here change little if the threshold number of points is decreased to 2 or increased to 8.

From these binned averaged densities, the geostrophic transport is calculated assuming a level of no motion at 170 m. This depth is about 20 m shallower than the depths of the sills separating the basins. This estimate of a level of no motion is roughly consistent with that used in past observations (Brown and Irish, 1992; Brooks and Townsend, 1989), and it is also consistent with the numerical model results. In Fig. 7, the seasonal cycle of transport across the sections connecting the deep basins of the GoM from the numerical model (with no wind forcing and monthly climatological density) are compared to estimates of geostrophic transport calculated from the density profiles in the numerical model at the endpoints of the sections. The seasonal cycle of the actual transport and the geostrophic estimate of transport agree well for the transport across the section between Jordan and Georges Basins ($r = 0.82$), and Jordan and Wilkinson Basins ($r = 0.73$). There is poor agreement ($r = -0.15$) in the seasonal cycle of the transport between Wilkinson and Georges Basins, though the overall magnitude agrees well. This disagreement is due to the seasonal variation in the SS inflow, which, as can be seen in Fig. 4, affects flow across this section. This is confirmed in numerical model runs in which inflow from the SS is blocked. In these runs, there is good agreement between the modeled and geostrophic transports between Wilkinson and Georges Basins. Regardless of the SS inflow, however, an anomaly in the density gradient

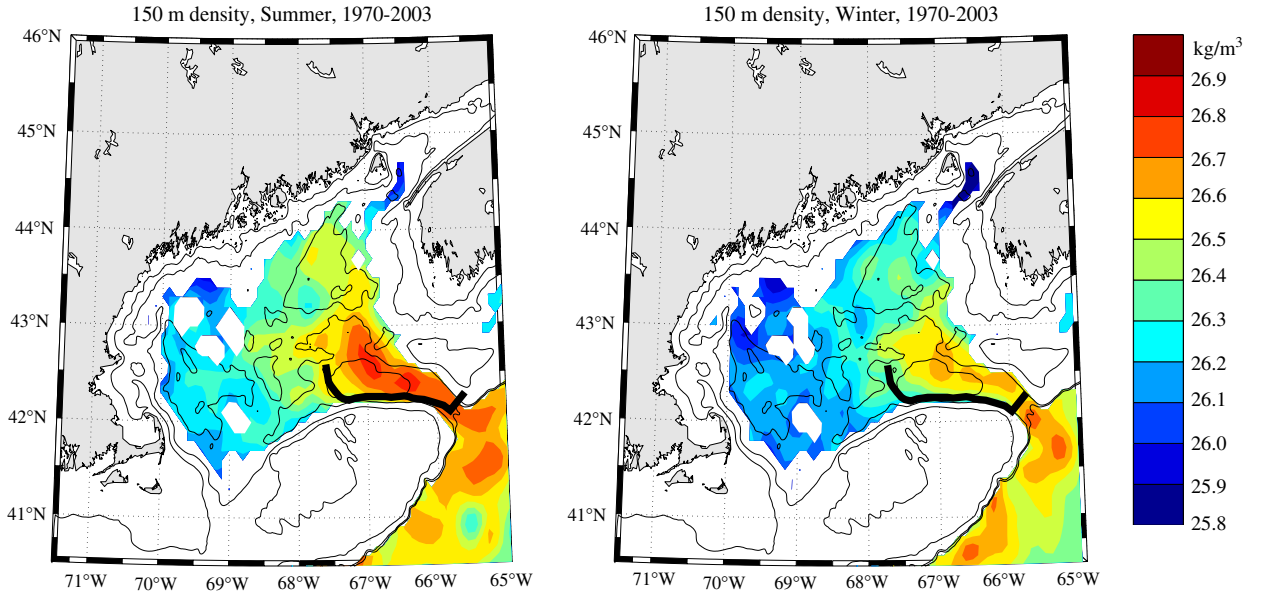

Fig. 6. Mean density at 150 m for (left) July–October and (right) January–April for the years 1970–2003, using all data from the BIO database. The thick black line around the south and west portions of Georges Basin mark the boundary of the area included in the density averages. Elsewhere along the perimeter of Georges Basin, the 200 m isobath is the limit of the averaging area, as it is in Wilkinson and Jordan Basins. The 300-, 200-, 100- and 50-m isobaths also are shown.

between Wilkinson and Georges Basins would drive an anomalous transport across the section connecting the basins.

As can be seen in Fig. 8, the density differences that drive the transport are at a maximum at depth, and are much reduced or even reversed near the surface, and thus it is the deep density gradients that drive the majority of the transport.

The decorrelation timescale of the geostrophic transport anomaly was calculated from quarterly estimates of the geostrophic transport. The seasonal cycle and a linear trend were first removed from these time series. The decorrelation time for the transport between Wilkinson Basin and Georges Basin was between a year and a year and half (with roughly $N = 40$ data points in each correlation). The decorrelation time for the transport across the section connecting Georges Basin and Jordan Basin is about a $\frac{3}{4}$ of a year (with N about 20 for each correlation). The decorrelation time for the transport across the section between Jordan Basin and Wilkinson Basin is difficult to resolve with quarterly data; when the analysis is repeated on bimonthly data, the timescale is about 4 months, but this is dependent on assuming that a single CTD cast in the basin in a monthly period is sufficient to characterize its density. The estimate of the decorrelation timescale in the geostrophic flow between Jordan Basin and Wilkinson Basin cannot be considered robust.

The SD of the transport is (Table 2) higher in the winter (quarter 1) than in the summer. The dispersion of the transport (Table 1) is correspondingly greater in the winter than the summer, but in either case, the dispersion of the transport driven by density changes is much greater than that driven by other sources of variability. Thus, on timescales of several months and longer, the transport variability driven by changes in hydrography dominates the other sources of variability. The implications of this finding to the predictability and modeling of the GoM flows are discussed below.

5. Discussion

The interannual variability of the density differences between the deep basins of the GoM is shown above to cause the large majority of the variability in the time-integrated transport in the central GoM on longer timescales. But these density differences are, of course, not a phenomenon external to the GoM. They are forced by the surface fluxes acting upon and the inflows into the GoM. In the following sections, the sources of these density

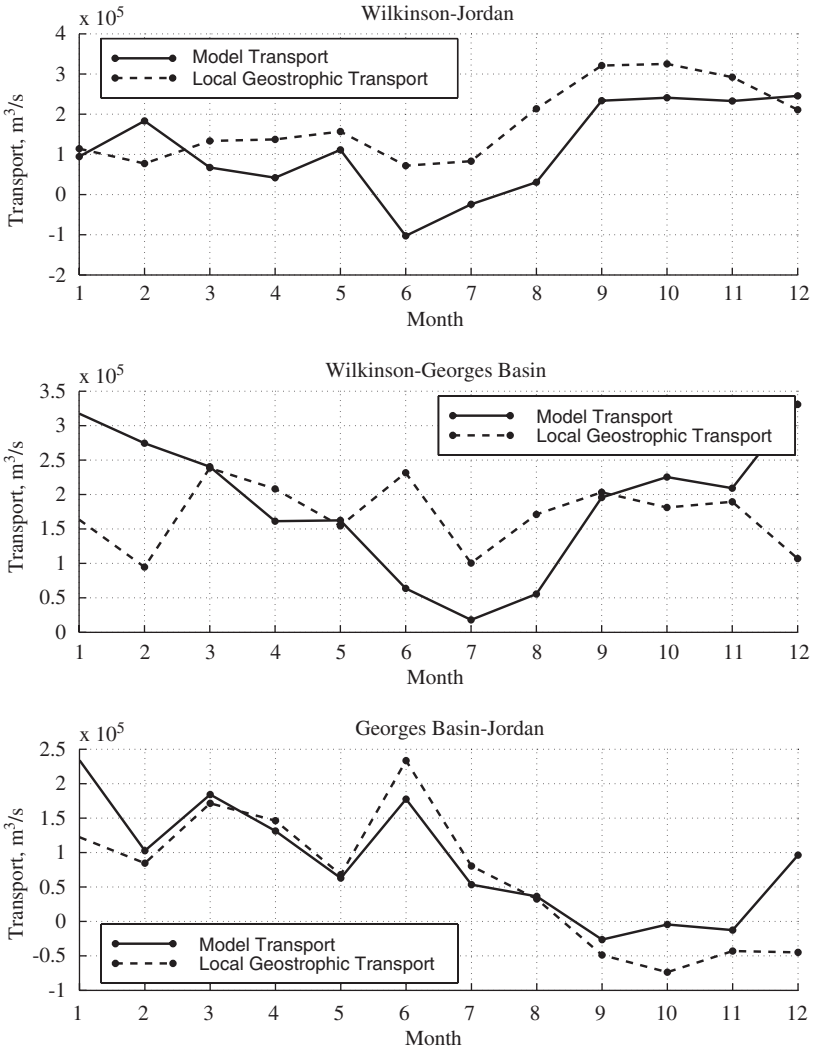

Fig. 7. Transport from the numerical model for the sections connecting the deep basins, and the equivalent geostrophic transport calculated from the density difference in the model between the basins, with a level of no motion at 170 m. (Top) Transport between Wilkinson and Jordan Basins. (Middle) Transport between Wilkinson and Georges Basins. (Bottom) Transport between Georges and Jordan Basins.

differences will be briefly examined, and from this understanding recommendations of the observations needed to understand and model the circulation in the central GoM will be made.

5.1. Origin of large-scale density differences in the GoM

The mean circulation in the GoM is counterclockwise, with water entering from the NEC and SS flowing from Georges Basin to Jordan Basin and then to Wilkinson Basin and then out of the GoM either through the Great South Channel, the NEC, or over the north flank of Georges Bank (Brown and Beardsley, 1978; Smith et al., 2001; Hopkins and Garfield, 1979). The density in the basins at depths below 50 m decreases as the water flows around the basins, with the lowest deep densities in Wilkinson Basin (Fig. 8; Smith et al., 2001). This decrease in density is associated with deep freshening and cooling, as the warm salty water entering the GoM through the NEC at depth is mixed during winter mixing events with cooler and fresher surface waters from the SS and from estuarine outflows (Brown and Beardsley, 1978; Smith et al., 2001).

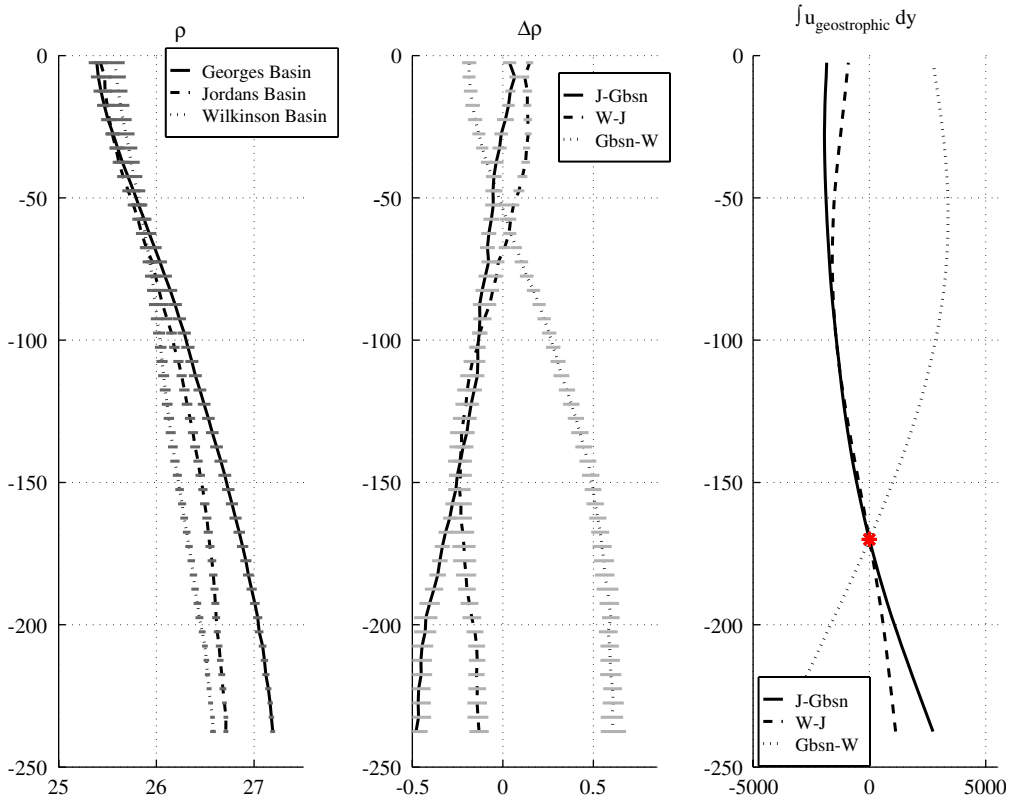

Fig. 8. Mean hydrography of the deep basins, averaged with all data from January to April for years 1970–2003. (Left) Density in the deep basins. Error bars indicate ± one standard error in the average density. (Middle) Density difference between two basins. Error bars indicate ± one standard error in the average density difference. (Right) Horizontal integral of geostrophic velocity between two basins, with level of no motion marked by asterisk at 170 m. Integrated transports and density differences do not sum exactly to zero because means are calculated over slightly different years, due to different missing years in the data for each basin.

Table 2
The mean and standard deviation of the geostrophic transport across the sections connecting the basins, and the number of years which contributed to each estimate

	Georges–Jordan (10^5 m^3 s^{-1})	Jordan–Wilkinson (10^5 m^3 s^{-1})	Wilkinson–Georges (10^5 m^3 s^{-1})
Mean			
Summer	−0.94	−3.28	4.26
Winter	−0.99	−1.56	2.21
Standard deviation			
Summer	1.27	1.32	1.46
Winter	1.52	2.16	2.13
Number of years in average			
Summer	22	20	22
Winter	13	11	17

Units are in m^3 s^{-1}. The means do not sum to zero for slightly different years contribute to each estimate, according to the availability of data in each basin and in each year. Each yearly estimate of the transport is independent, or nearly so, so the standard error in the mean should be approximately the standard deviation of the transport divided by the square root of the number of years which contribute to the data. Summer is defined here as July through October, and Winter as January through April.

The climatological cycles of density, temperature and salinity suggest that both winter fluxes of heat and momentum are important contributers to vertical mixing. Xue et al. (2000) found that much of the circulation in the GoM is driven by buoyancy fluxes, especially around the perimeter of the GoM. However, the water mass alterations experienced by the water moving through the central GoM are not consistent with mixing driven by surface cooling alone. When cooling or evaporation drives vertical mixing, the entire mixed water column becomes denser. When vertical mixing is driven by surface-forced mechanical turbulence, deeper waters become less dense, and surface waters denser, as the water column is homogenized.

In a monthly climatology (Fig. 9) of the density of Wilkinson Basin, the waters below 100 m are freshest, coolest and least dense at the end of the winter. Furthermore, as the deep waters circulate counter-clockwise through the GoM, they get steadily less dense. Thus mechanical mixing, presumably driven at least in part by winter storms, must be an important contributer to the deep mixing. This is not to say surface buoyancy loss is unimportant: the surface waters are coldest at the end of the winter, and this contributes significantly to their densification. (A vertically homogeneous water column is not seen in the climatology to the full depth of the apparent effect of winter-time mixing because the climatology is an average over years with deep mixing and years without. The later years will contribute an average stratification to the deep waters in the climatology.)

The other basins show similar but weaker seasonal cycles of density as a function of depth, but their climatological stratification remains much stronger. This suggests that deep winter-time mixing is much less common in the other basins than in Wilkinson Basin, which agrees well with prior analysis (Hopkins and Garfield, 1979; Brown and Beardsley, 1978).

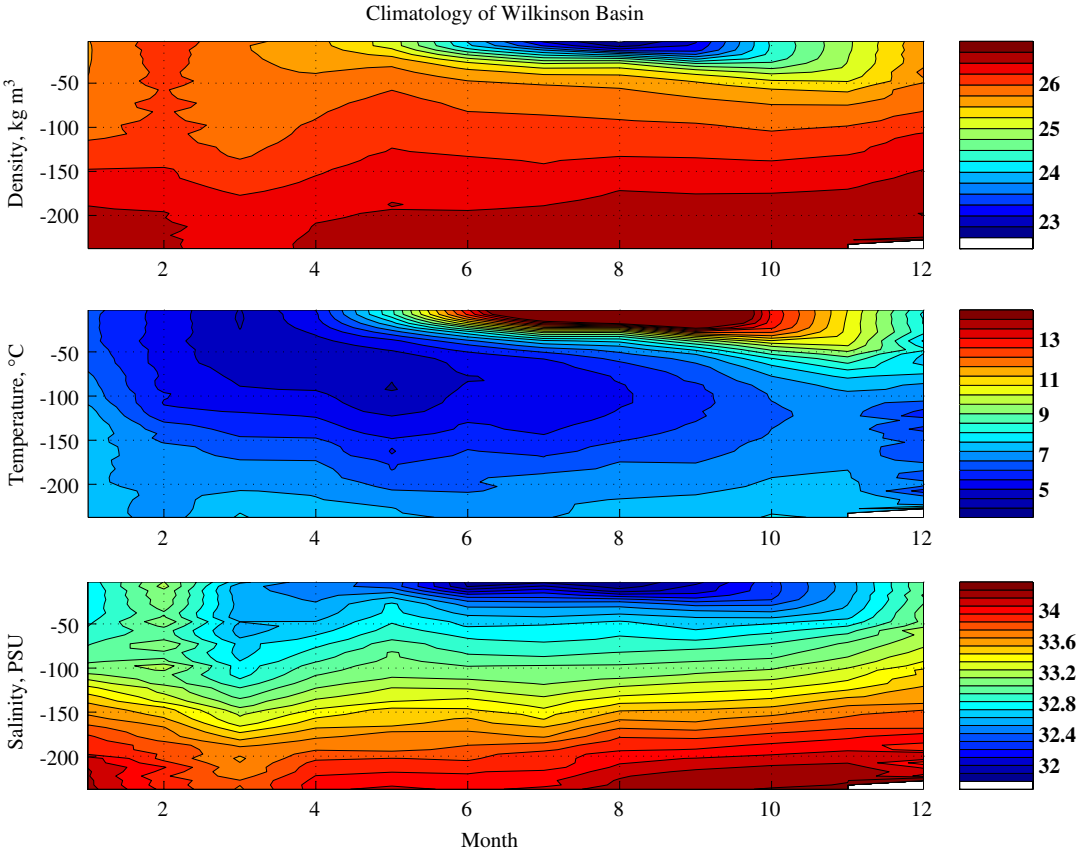

Fig. 9. The monthly climatology of density, temperature and salinity in Wilkinson Basin from the BIO hydrographic database, including all data from 1970 to 2003. Density and salinity inversions in the upper 100 m in February are a result of changes in vertical sampling resolution between the beginning and end of the data period.

A qualitative estimate of the relative importance of surface cooling and wind-driven mixing to the variability in the density gradients in the central Gulf can be found by comparing the density and density differences in and between Wilkinson Basin and Georges Basin to the surface fluxes of heat and momentum. (Jordan Basin is excluded from this analysis because its relatively poor data coverage reduces the power of the statistical analysis there). Comparisons were made between the density and density differences averaged from May to July and the integrated surface heat fluxes and the integrated absolute value of windstress for the preceding January through March. The time lag between the fluxes and the density was introduced in order to capture the full effect of the mixing (e.g., January densities do not incorporate the effects of March winds) and to take advantage of the greater oceanic data coverage in the summer. The strength of the wind mixing was estimated from the integrated absolute value of the windstress from the NCEP reanalysis (Kalnay et al., 1996). Using the integral of stress raised to the three-halves power (e.g., u^{*^3}) made little difference. The mixing effects of buoyancy fluxes were estimated from the integrated surface heat fluxes from the NCEP reanalysis as well. This product is known to over-estimate latent and sensible heat fluxes (Renfrew et al., 2002). However, comparison of the fluxes with in situ estimates over the period of February–April 1995 (Beardsley et al., 2003; data courtesy of Beardsley) finds that the correlation between the total heat flux and NCEP fluxes, both low passed with a 3-day filter, is 0.95. This indicates that the NCEP fluxes capture the variability in the surface buoyancy fluxes very well.

The density in Wilkinson Basin is significantly positively correlated with winter cooling from 30- to 170-m depth with a peak correlation of about 0.7 between 60 and 150 m (the surface 30 m has been warmed by the summer sun). The density in Georges Basin is more weakly correlated to the integrated cooling, and the significant correlation between cooling and density is limited to the top 90 m of the water column, again suggesting limited deep mixing in this basin. Thus the density difference between the two basins is negatively correlated to the net cooling (peak correlation of $r = -0.6$ from 150 to 50 m), with greater cooling reducing the density difference between the two basins. The geostrophic transport across the section connecting the two basins, as calculated above, is significantly correlated to the net cooling with more cooling resulting in less transport ($r = -0.6$). All correlations greater than $r = 0.42$ are significant at $P < 0.05$ with 21 degrees of freedom from 21 years in which both basins had at least four casts within the basin in the months of interest.

There is a similar relation between integrated windstress and inter-basin density differences, but the correlations are weaker. The density in Wilkinson Basin is weakly but positively correlated to the strength of the integrated winter windstress magnitudes from 30- to 150-m depth, while the positive correlation in Georges Basin is limited to the surface 80 m. The density differences between the basins is only weakly correlated to the integrated windstress from 110 to 200 m, and then with only marginal significance ($r = 0.43$). The geostrophic transport is not significantly correlated to the strength of wind mixing ($r = 0.25$).

The correlations of cooling and integrated windstress magnitude with between-basin density differences are consistent with a model of deep mixing in Wilkinson Basin setting up deep density contrasts with Georges Basin, which then drive cross-Gulf transports. Winter time vector-mean alongshore and cross-shore winds are not correlated to the geostrophic transports, suggesting that mean wind-driven transports are not important drivers of inter-basin density differences. Nor are the density or density differences between basins correlated to the peak windstress magnitudes in each winter.

The relative unimportance of interannual changes in integrated windstress magnitude to the interannual changes in horizontal density gradients, despite the importance of mechanical mixing to the evolution of the mean vertical density structure described above, perhaps can be explained by the relative lack of variability in the time-integrated windstress magnitude. The ratio of the SD to the mean integrated windstress magnitude is about 6%, while the same ratio for the integrated cooling is 28%. Thus while the wind mixing is important, its relative constancy means it does not contribute as significantly to year-to-year changes in the vertical mixing of the water column or to the variation in the horizontal density gradients. Also, much of the mechanical mixing may be caused by the strong tides in the GoM, and especially in Jordan Basin, and this will have little variability from year to year (Brooks and Townsend, 1989).

Neither the variation in the winds nor the surface cooling explains a great deal of the variance in the

density difference between the basins, or in the geostrophic transport these density differences drive. At most, year-to-year variation in cooling explains about 36% of the variability in the geostrophic transport between Georges Basin and Wilkinson Basin. The rest of the variability is likely to arise from two sources. First, time variation in the density of the waters flowing into the GoM will translate into density differences between the basins until water with the new density is able to flow into all of the basins. Second, a change in the stratification of the waters entering the GoM through the NEC or the SS, or a change in the density differences between these two inflows, could modulate the stratification in the basins, and thus ability of the winds or cooling to mix the waters. To understand these sources of variability, we must sample these inflows on the timescales needed to resolve the fluctuations in their heat and freshwater transport.

5.2. *What must be observed to explain GoM circulation variability?*

The majority of the variability in the central GoM circulation averaged over several months and longer timescales is driven by the fluctuation of density gradients in the GoM. To model this circulation and its fluctuations successfully, the evolution of these gradients must be captured by the model or imposed by the data used to constrain the model solution. Two approaches exist, neither of which are mutually exclusive.

A model able to run for the timescale of water residence in the GoM could be forced by the observed surface heat and buoyancy fluxes and by observations of the density of the water entering through the NEC and the SS. The main obstacle to such a model is the lack of measurements in the SS and the NEC of sufficient spatial and temporal density. In the absence of detailed knowledge of the inflows, or in the absence of confidence in the ability of the model and forcing to capture mixing processes accurately, some form of data assimilation must be used to constrain the large-scale density field in the model.

Recent efforts at modeling the GoM have assimilated sea-surface temperature (SST) by nudging the model surface temperature toward observations (Chen et al., 2006; H.J. Xue, pers. com.). However, a brief consideration of the thermal structure of the GoM suggests that this may not be useful in constraining the extent of vertical mixing in the winter. In most oceans, temperature decreases with depth, so excess deepening of the mixed layer will over-cool the surface, while insufficient deepening of the mixed layer will leave the surface warmer than it should be. Nudging the surface temperature toward the observed value will cool the surface if the mixed layer is too shallow, increasing mixing, and will warm the surface if the mixed layer is too deep, inhibiting mixing. Thus, nudging will tend to correct the model errors in an ocean with a more typical vertical temperature distribution. However, in the GoM, temperature increases with depth below the seasonal thermocline. Over deepening the mixed layer will make the surface anomalously warm, while a too-shallow mixed layer will leave the surface colder than it should be. Nudging the SST to the observed SST will thus tend to cause the model to mix less if the mixed layer is too shallow, and mix more if the mixed layer is too deep. Thus, the incorporation of SST into the model with nudging will not tend to correct any problem the model might have with vertical mixing in the winter. It is unlikely that any more advanced data assimilation scheme would tend to do better, for in the absence of surface salinity data it is not possible to unambiguously ascribe any error in vertical mixing to insufficient surface cooling, erroneous deep temperature/salinity structure, or the model incorrectly parameterizing mixing. No assimilation scheme can remove ambiguity from a poorly observed system.

If data assimilation is to be used to constrain a GoM circulation model, we must observe density in the basins at the deeper depths where the density gradients that drive the geostrophic transport exist. The necessary frequency of sampling is set by the decorrelation timescales of the density in the basin. As shown in Table 3, the decorrelation timescale of density after the removal of the seasonal cycle ranges from 0.27 years in the deep Georges Basin to

Table 3
Decorrelation timescale in years for density in the deep basins in the GoM as a function of depth

Depth (m)	Georges Basin (years)	Jordan Basin (years)	Wilkinson Basin (years)
10	0.62	0.57	0.31
50	0.50	0.72	0.57
100	0.43	0.54	0.89
150	0.30	0.54	0.89
200	0.27	0.56	0.75

The seasonal cycle was removed before making the calculation.

half a year or more in the mid-depths of the basins (see Ramp et al., 1985 on rapid change in the T/S properties of water entering through the NEC). Thus quarterly monitoring of the density in the deep basins could begin to provide the data needed to constrain the modeled circulation of the central GoM through the assimilation of the deep density structure in the basins.

6. Conclusions

The variability in the time-integrated transport on timescales of several months and larger in the GoM is driven largely by changes in the density structure (at least in the interior of the GoM), and to a lesser extent by the SS inflow, and finally by the winds. However, neither the observations needed to accurately capture the SS inflow variability, nor the information needed to capture the variation in the internal density structure of the GoM have been made sufficiently often to meaningfully constrain the models. Thus our models will fail to inform us of the nature of the true variability of the GoM circulation, no matter how perfect the models themselves are.

If the year-to-year variation in the circulation of the GoM is to be understood and quantified, its boundaries must be routinely monitored. The volume of water entering the GoM from the NEC and the SS must be recorded on timescales short compared to the variability of the inflow (about 10 days). More importantly, the density of the waters entering the GoM at depth and near the surface, in the SS and through the NEC, must be routinely observed. If this cannot be done with sufficient frequency, the density within the GoM must be monitored at least once a quarter to constrain the circulation in the central GoM through data assimilation. If we can afford only one of these methods, measuring the inflows is preferable for it would allow us to understand why the GoM circulation is changing, and could perhaps be used to understand these changes before they happen.

The scarcity of hydrographic data prevented similar calculations from being made for the Maine coastal currents, but it also seems likely that much of the variability in their transport is a function of changes in the density field that are poorly constrained in present models (e.g., Brooks, 1994; Hetland and Signell, 2005; Xue et al., 2000; Pettigrew et al., 2005). Thus there is, at present, a mismatch between what we know and observe and what we must know and observe if we are to understand the variations in GoM circulation. No further refinements in our numerical models will be as useful as an effort to improve the observations that drive the models. Efforts have begun to measure the relevant data, for example the moorings monitoring the NEC and SS inflow maintained by the Gulf of Maine Ocean Observing System (http://www.gomoos.org/), and the routine salinity/temperature measurements made by the National Marine Fisheries Service (Taylor and Bascunan, 2000). These must be maintained if we are to understand the year-to-year variation in the GoM circulation and its effects on the ecosystem of the Gulf.

Acknowledgments

This paper is stronger for helpful comments of Ken Brink, Dave Mountain, Bob Beardsley and many others who commented on it in various GLOBEC meetings. It would not be possible without Changsheng Chen's excellent development of FVCOM for the Gulf of Maine. It is based on data from many groups, including all who contributed their data to the hydrographic database maintained by the Bedford Institute of Oceanography. It was funded by NSF OCE-0219709, and is GLOBEC contribution no. 308.

Appendix A

The GoM is numerically modeled with the FVCOM. FVCOM is a free-surface, hydrostatic, primitive-equation numerical model with an unstructured triangle-based finite element mesh (Chen et al., 2003). The model was configured to the GoM as described by Chen et al. (2006). The model mesh, shown in Fig. 1, has a resolution of about 8 km in the central GoM, reducing to 1.4–4 km on the steep portions of the northeast flank of Georges Bank and in coastal regions where the bathymetry has the shortest lengthscales. The depth of the slope and ocean outside of the GoM is truncated to 300 m to reduce the computational demands on the model, and cross-comparison with full depth models indicates that this does not effect the results presented below (Chen et al., 2006), though it does reduce the magnitude of the flows along the slope by removing the deep density gradients that drive them. The bathymetry is not truncated within the GoM.

The model is initialized at each month with a climatological monthly mean density field, described by Chen et al. (2006). Because of the increase in hydrographic data density at later dates, this climatological density field is heavily biased toward the past decade, with 68% of the data from 1990 to the present.

The wind forcing of the GoM is coherent over the model domain. On the 2–14 day timescales over which the GoM responds most strongly and coherently to wind forcing, the vector correlation coefficient between the National Center for Environmental Prediction (NCEP) winds (Kalnay et al., 1996) in the central Gulf of Maine and on the model boundaries is greater than 0.8 everywhere, and the magnitude of the correlated part of the winds varies relatively little over the model domain (cf. Noble et al., 1985; Brown, 1998 on the GoM wind response; and Chen et al., 2006; Manning and Strout, 2001 on the extent and effects of spatially varying winds in the GoM). Thus, the model is forced by a uniform windstress whose magnitude and direction is equal to the NCEP reanalysis windstress at 42.8°N and 67.5°W, roughly in the center of Georges Basin. The NCEP winds compare well to observations (Manning and Strout, 2001) and in comparison to Beardsley in situ flux estimates on the South Flank of Georges Bank (cf. Fig. 2.). Uniform winds also have been used in most prior modeling (Greenberg et al., 1997; Hannah et al., 2001; Naimie et al., 1994, but for exceptions see Chen et al., 2005; Brown, 1998).

The winds force circulation not only in the GoM and SS system, but, because of the long length scales of the winds, they also force circulation outside of the model domain, which can affect the model solutions through the open boundary. These effects are most important on the SS, for it is the boundary from which coastal trapped waves can enter the domain. In order to capture these effects, the free surface at the SS open boundary was modified to reflect the coastal setup/setdown driven by alongshore winds as observed by Schwing (1989) as part of the CASP. The setup was calculated from their observations, interpolated to their kilometer 300, which is the location of the SS open boundary in FVCOM. The cross-SS windstress was found to have a negligible impact on the coastal sea-level, so its effects on the elevation on the open boundary was neglected. Schwing (1989) calculated that a 1 Pa wind along the SS (i.e. from 68°T) would lead to a 50-cm rise in sea-level at the coast at the location of the model open boundary (from Schwing's, 1989 "L" model, which implicitly includes the effects of the winds on the SS and the winds to the northeast which are correlated with these winds). Unfortunately, the observations of wind-driven setup/setdown from CASP do not greatly constrain the cross-shelf structure of the sea-level signal. This structure determines the transport driven across the boundary by the winds. As can be seen in Fig. 1, the bathymetry at the boundary slopes to a maximum depth about a third of the way across the shelf, and then rises onto Emerald Bank before reaching the shelf break and slope. Any cross-shelf gradient in sea-level imposed on the Bank drives a circulation, which in the model joins the coastal transport, though in reality it is likely that little surface pressure gradient would be wind-forced on such a bank (Brink, 1983). Any cross-shelf gradient imposed on the open boundary offshore of the Bank joins a slope circulation which has little impact on the GoM. We choose to impose the free-surface cross-shelf gradient associated with the along SS wind linearly from the coast to the deepest point of the offshore basin, with a uniform free-surface offshore of this point. This is roughly consistent with the observations of sea-surface pressure change across the shelf at Halifax as observed by Schwing (1989). Spreading the wind-forced cross-shelf sea-surface gradient at the boundary farther offshore would tend to decrease the impact of alongshore winds on the GoM by moving more of the wind-driven circulation onto the slope. Whether this is appropriate must be determined by further modeling or observation.

For the model runs used to estimate the transfer coefficients between wind and transport in the GoM, the model was spun-up with no winds for 10 tidal cycles (similar to Naimie, 1996; Hannah et al., 2001), and then the winds were applied at half strength for half an inertial period and then full strength for 3.6 more days. This stepped forcing nearly eliminates inertial oscillations forced by the onset of the winds. The duration of forcing is within the times over which Noble et al. (1985) and Brown (1998) found the maximum coherence between winds and currents. The transfer function between winds and currents is only slightly changed if these results are calculated with a wind stress 50% greater or smaller, and is also only weakly affected if the winds are run at full strength for 2 or 7 days.

Besides the winds, transports through the SS boundary can be forced by cross-shelf density and

steric height gradients along the open boundary (Schwing, 1989; Anderson and Smith, 1989; Smith and Schwing, 1991). The alongshelf transport across the SS boundary forced by cross-shelf density gradients depends on the choice of a level of no motion. The nearly universal practice on the SS has been to assume that the cross-shelf pressure gradient caused by the hydrography, and thus the alongshelf geostrophic flow, is zero at the bottom. Thus the level of no motion is the water depth (Hannah et al., 1998, 2001; Hetland and Signell, 2005; Han and Loder, 2003; Naimie, 1996). The alongshelf transport across the open boundary is calculated by the model and is consistent with thermal wind. This, in turn, is consistent with observations of the vertical shear of alongshelf currents on the SS (Anderson and Smith, 1989).

The variability in the SS inflow to the model driven by changes in the cross-shelf density gradient will be simulated by varying the sea-surface pressure along the boundary. On timescales less than that needed to advect density from the boundary to the interior of the model domain, this essentially barotropic forcing has been confirmed in model runs to produce the same effect on the interior of the model as changing the cross-shelf density gradient on the boundary of the model. The longer timescale changes in the density field on the SS and in the GoM driven by changes in the inflow are considered elsewhere, as part of the examination of variability driven by changes in the density field. Changing the boundary inflow changes the flow field of the model within a day and a half. As with the winds, models run with modified boundary conditions are run with the unaltered boundary conditions for 10 tidal cycles and then the altered boundary conditions is imposed over two steps a half-inertial period apart, and then held steady for 3.6 days. The transfer function between the altered SS inflow and the circulation in the model are computed from the last tidal cycle of this period. The results are little changed if the period of the altered flow is increased to the decorrelation period defined below for the SS inflow variability.

Attempts were made to alter the volume of water entering the GoM through the NEC in the model by changing the alongshelf break flow entering the model domain through the northeastern open boundary, and by changing the baroclinicly forced shelfbreak current. Neither of these made significant changes to the NEC inflow. Only by changing the wind field, the SS inflow, or the density field in the GoM was it possible to alter the inflow and outflow through the NEC (consistent with Ramp et al., 1985). It seems that the circulation through the NEC is a function of the forcing on the GoM, and thus that this inflow is controlled by the GoM. Of course, the heat and freshwater transport through the NEC is influenced by the water properties at its mouth.

The open boundary conditions and the data used to forced the M_2 tides, and the details of the open boundary conditions on the Mid-Atlantic Bight and the offshore ocean, can be found in Chen et al. (2006).

References

Anderson, C., Smith, P., 1989. Oceanographic observations on the Scotian Shelf during CASP. Atmosphere-Ocean 27 (1), 130–156.

Beardsley, R., Lentz, S., Weller, R., Limeburner, R., Irish, J., Edson, J., 2003. Surface forcing on the southern flank of Georges Bank, February–August 1995. Journal of Geophysical Research 108 (C11).

Bevington, P.R., Robinson, D.K., 1992. Data Reduction and Error Analysis for the Physical Sciences. McGraw-Hill, New York.

Bracewell, R.N., 1986. The Fourier Transform and Its Applications. McGraw-Hill, New York.

Brink, K., 1983. Low-frequency free wave and wind-driven motions over a submarine bank. Journal of Physical Oceanography 13 (1), 103–116.

Brooks, D., 1994. A model study of the buoyancy-driven circulation in the Gulf of Maine. Journal of Physical Oceanography 24 (11), 2387–2412.

Brooks, D., Townsend, D., 1989. Variability of the coastal current and nutrient pathways in the Eastern Gulf of Maine. Journal of Marine Research 47 (2), 303–321.

Brown, W., 1998. Wind-forced pressure response of the Gulf of Maine. Journal of Geophysical Research 103 (C13), 30,661–30,678.

Brown, W., Irish, J., 1992. The annual evolution of geostrophic flow in the Gulf of Maine: 1986–1987. Journal of Physical Oceanography 22, 445–473.

Brown, W.S., Beardsley, R.C., 1978. Winter circulation in the Western Gulf of Maine, part I, cooling and water mass formation. Journal of Physical Oceanography 8, 265–277.

Byers, J., Pringle, J., 2006. Going against the flow: range limits and invasions in advective environments. Marine Ecology Progress Series 313, 27–41.

Chen, C., Beardsley, R., Limeburner, R., 1995. A numerical study of stratified tidal rectification over finite amplitude banks 2: Georges-Bank. Journal of Physical Oceanography 25 (9), 2111–2128.

Chen, C., Liu, H., Beardsley, R., 2003. An unstructured grid, finite-volume, three-dimensional, primitive equations ocean model: application to coastal ocean and estuaries. Journal of Atmospheric and Oceanic Technology 20 (1), 159–186.

Chen, C., Beardsley, R.C., Hu, S., Xu, Q., Lin, H., 2005. Using MM5 to hindcast the ocean surface forcing fields over the

Gulf of Maine and Georges Bank region. Journal of Atmospheric and Oceanic Technology 22, 131–145.

Chen, C., Beardsley, R.C., Xu, Q., Cowles, G., Limeburner, R., 2006. Tidal dynamics in the Gulf of Maine and New England shelf: an application of FVCOM. Journal of Geophysical Research, in revision.

Davis, R., 1976. Predictability of sea surface temperature and sea level pressure anomalies over the North Pacific Ocean. Journal of Physical Oceanography 6, 249.

Dever, E., 1997. Wind-forced cross-shelf circulation on the Northern California Shelf. Journal of Physical Oceanography 27, 1566–1579.

Franks, P., Anderson, D., 1992. Alongshore transport of a toxic phytoplankton bloom in a bouyancy current—*Alexandrium tamarense* in the Gulf of Maine. Marine Biology 112 (1), 153–164.

Greenberg, D., Loder, J., Shen, Y., Lynch, D., Naimie, C., 1997. Spatial and temporal structure of the barotropic response of the Scotian Shelf and Gulf of Maine to surface wind stress: a model-based study. Journal of Geophysical Research 102 (C9), 20,897–20,915.

Han, G., Loder, J., 2003. Three-dimensional seasonal-mean circulation and hydrography on the Eastern Scotian Shelf. Journal of Geophysical Research 108 (C5).

Hannah, C., Naimie, C., Loder, J., Werner, F., 1998. Upper-ocean transport mechanisms from the Gulf of Maine to Georges Bank, with implications for *Calanus* supply. Continental Shelf Research 17, 1887–1911.

Hannah, C., Shore, J., Loder, J., Naimie, C., 2001. Seasonal circulation on the Western and Central Scotian Shelf. Journal of Physical Oceanography 31 (2), 591–615.

Hetland, R., Signell, R., 2005. Modeling coastal current transport in the Gulf of Maine. Deep-Sea Research II 52(19–21), 2430–2449.

Hopkins, T., Garfield, N., 1979. Gulf of Maine intermediate water. Journal of Marine Research 37 (1), 103–139.

Johnson, C., Pringle, J., Chen, C., 2006. Transport and retention of dormant copepods in the Gulf of Maine. Deep-Sea Research II, this issue [doi:10.1016/j.dsr2.2006.08.016].

Kalnay, E., Kanamitsu, M., Kistler, R., Collins, W., Deaven, D., Gandin, L., Iredell, M., Saha, S., White, G., Woollen, J., Zhu, Y., Chelliah, M., Ebisuzaki, W., Higgins, W., Janowiak, J., Mo, K., Ropelewski, C., Leetmaa, A., Reynolds, R., Jenne, R., 1996. The NCEP/NCAR 40-year reanalysis project. Bulletin of the American Meteorological Society 77, 437–471.

Large, W., Pond, S., 1981. Open ocean momentum flux measurements in moderate to strong winds. Journal of Physical Oceanography 11, 324–336.

Loder, J., Hannah, C., Petrie, P., Gonzalez, E., 2003. Hydrographic and transport variability on the Halifax section. Journal of Geophysical Research 108 (C11).

Manning, J., Strout, G., 2001. Georges Bank winds: 1975–1997. Deep-Sea Research II 1–3, 115–135.

Naimie, C., 1996. Georges Bank residual circulation during weak and strong stratification periods: prognostic numerical model results. Journal of Geophysical Research 101 (C3), 6469–6486.

Naimie, C., Loder, J., Lynch, D., 1994. Seasonal-variation of the 3-dimensional residual circulation on Georges Bank. Journal of Geophysical Research 99 (C8), 15,967–15,989.

Noble, M., Butman, B., Wimbush, M., 1985. Wind-current coupling on the southern flank of Georges Bank—variation with season and frequency. Journal of Physical Oceanography 15 (5), 604–620.

Pettigrew, N., Churchill, J., Janzen, C., Mangum, L., Signell, R., Thomas, A., Townsend, D., Wallinga, J., Xue, H., 2005. The kinematic and hydrographic structure of the Gulf of Maine coastal current. Deep-Sea Research II 52 (19–21), 2369–2391.

Ramp, S., Schlitz, R., Wright, W., 1985. The deep flow through the Northeast Channel, Gulf of Maine. Journal of Physical Oceanography 15 (12), 1790–1808.

Renfrew, I., Moore, G., Guest, P., Bumke, K., 2002. A comparison of surface layer and surface turbulent flux observations over the Labrador sea with ECMWF analyses and NCEP reanalyses. Journal of Physical Oceanography 32 (2), 383–400.

Roworth, E., Signell, R., 1998. Construction of digital bathymetry for the Gulf of Maine. OPEN-FILE REPORT 98-801, Coastal and Marine Geology Program.

Schwing, F.B., 1989. Subtidal response of the Scotian Shelf bottom pressure field to meteorological forcing. Atmosphere-Ocean 27, 157–180.

Smith, P., Schwing, F., 1991. Mean circulation and variability on the Eastern Canadian Continental Shelf. Continental Shelf Research (8–10), 977–1012.

Smith, P., Houghton, R., Fairbanks, R., Mountain, D., 2001. Interannual variability of boundary fluxes and water mass properties in the Gulf of Maine and on Georges Bank: 1993–1997. Deep-Sea Research II 48 (1–3), 37–70.

Taylor, M., Bascunan, C., 2000. CTD data collection on Northeast Fisheries Science Center cruises: standard operating procedures. National Marine Fisheries Service, Northeast Fisheries Science Center Reference Doc. 00-11.

Vermersch, J., Beardsley, R., Brown, W., 1979. Winter circulation in the Western Gulf of Maine: 2 current and pressure observations. Journal of Physical Oceanography 9 (4), 768–784.

Xue, H., Chai, F., Pettigrew, N., 2000. A model study of the seasonal circulation in the Gulf of Maine. Journal of Physical Oceanography 30 (5), 1111–1135.